A&A 623, A126 (2019)
https://doi.org/10.1051/0004-6361/201834993

Astronomy & Astrophysics

Effects of a revised ^{7}Be e$^-$-capture rate on solar neutrino fluxes*

D. Vescovi[1,2], L. Piersanti[3,2], S. Cristallo[3,2], M. Busso[4,2], F. Vissani[5], S. Palmerini[4,2], S. Simonucci[6,2], and S. Taioli[7,8]

[1] Gran Sasso Science Institute, Viale Francesco Crispi, 7, 67100 L'Aquila, Italy
e-mail: diego.vescovi@gssi.it
[2] INFN, Section of Perugia, Via A. Pascoli snc, 06123 Perugia, Italy
[3] INAF, Observatory of Abruzzo, Via Mentore Maggini snc, 64100 Teramo, Italy
[4] University of Perugia, Department of Physics and Geology, Via A. Pascoli snc, 06123 Perugia, Italy
[5] INFN, Laboratori Nazionali del Gran Sasso, Via G. Acitelli, 22, Assergi, L'Aquila, Italy
[6] Division of physics School of Science and Technology Università di Camerino, Italy
[7] Faculty of Mathematics and Physics, Charles University, Prague, Czech Republic
[8] European Centre for Theoretical Studies in Nuclear Physics and Related Areas (ECT*-FBK) and Trento Institute for Fundamental Physics and Applications (TIFPA-INFN), Trento, Italy

Received 28 December 2018 / Accepted 4 February 2019

ABSTRACT

Context. Electron-capture on ^{7}Be is the main production channel for ^{7}Li in several astrophysical environments. Theoretical evaluations have to account for not only the nuclear interaction, but also the processes in the plasma in which ^{7}Be ions and electrons interact. In recent decades several estimates were presented, pointing out that the theoretical uncertainty in the rate is in general of a few percent.
Aims. In the framework of fundamental solar physics, we consider a recent evaluation for the ^{7}Be+e$^-$ rate, which has not been used up to now, in the estimate of neutrino fluxes.
Methods. We analyzed the effects of the new assumptions on standard solar models (SSMs) and compared the results obtained by adopting the revised ^{7}Be+e$^-$ rate to those obtained by that reported in a widely used compilation of reaction rates (ADE11).
Results. We found that new SSMs yield a maximum difference in the efficiency of the ^{7}Be channel of about −4% with respect to what is obtained with the previously adopted rate. This fact affects the production of neutrinos from ^{8}B, increasing the relative flux up to a maximum of 2.7%. Negligible variations are found for the physical and chemical properties of the computed solar models.
Conclusions. The agreement with the Sudbury Neutrino Observatory measurements of the neutral current component of the ^{8}B neutrino flux is improved.

Key words. neutrinos – nuclear reactions, nucleosynthesis, abundances – Sun: abundances – Sun: helioseismology – Sun: interior

1. Introduction

Solar models and their comparisons with observations are a powerful tool for probing the solar interiors with high accuracy, describing the trend of the sound speed, and predicting how neutrinos are distributed among the various channels (see, e.g., Bahcall et al. 2001, for a review).

Solar neutrino measurements in particular those from the ^{8}B channel (Aharmim et al. 2013; Abe et al. 2016) yielded information on fundamental neutrino properties; nowadays these properties are measured with an increasing accuracy and detailed knowledge of neutrino fluxes is also important to this aim.

Very recently the Borexino collaboration presented the first global analysis of three individual neutrino components of the proton–proton (pp) chain, namely pp, ^{7}Be, and pep neutrinos, also putting an upper limit for those from CNO, over an energy range from 0.19 MeV to 2.93 MeV (Agostini et al. 2018).

These new data on neutrino fluxes can be used to improve our knowledge of the solar interiors (Vinyoles et al. 2017), which is still beset with problems; among these, of special relevance are those raised by the compilations of solar abundances based on 3D atmospheric models (Asplund 2005), which lead to disagreements with the measured sound speed (Bahcall et al. 2005b).

Standard solar model predictions for neutrino fluxes are then very sensitive to the reaction rates adopted, obviously including electron-captures in the plasma (which are also of great importance for several other astrophysical problems). The electron-capture rate on ^{7}Be itself is strongly dependent on the density and temperature distribution in the stellar structure (Simonucci et al. 2013); in solar conditions, in particular, this destruction channel of ^{7}Be dominates over proton captures (Adelberger et al. 1998). From this latter branching, through ^{8}B-decays, further neutrinos are emitted and can be detected by experiments such as Super-Kamiokande, Sudbury Neutrino Observatory (SNO), and KamLand. The observed flux of ^{8}B neutrinos is expected to be inversely proportional to the electron-capture rate on ^{7}Be because the counting rate in experiments is determined by the number of proton-capture reactions occurring per unit of time (Bahcall & Moeller 1969). Despite many different estimates presented (Bahcall 1962; Bahcall & Moeller 1969; Johnson et al. 1992; Gruzinov & Bahcall 1997), the accuracy in our knowledge of the relative importance of these two channels in not yet satisfactory and improvements have been limited over the years.

In this work we make a step forward by using a new estimate of the electron-capture rate on ^{7}Be (Simonucci et al. 2013, hereafter STPB13) to compute standard solar models (SSMs).

* The electron-capture table is only available at the CDS via anonymous ftp to cdsarc.u-strasbg.fr (130.79.128.5) or via http://cdsarc.u-strasbg.fr/viz-bin/qcat?J/A+A/623/A126

The results are then compared with those obtained by the widely used rate by Adelberger et al. (2011; hereafter ADE11), focusing our attention on solar neutrino fluxes. We make use of a tabulated version of the decay rate by STPB13. The aforementioned table, available at the CDS, contains the following information. Column 1 lists the density over the mean molecular weight for electrons in units of g cm^{-3}, Col. 2 gives the temperature in units of K, and Col. 3 provides the value of the electron-capture rate in units of s^{-1}. All the quantities are expressed in logarithmic scale. We also present an analytical approximation to the electron-capture rate. Our work is organized as follows. In Sect. 2 the main features of the adopted stellar evolutionary code and of SSMs are described. Section 3 illustrates the calculation of the electron-capture rate on ^{7}Be and presents a comparison with the previous estimate. In Sect. 4 we analyze the main characteristics of the ensuing SSM, while in Sect. 5 the impact of the adopted rate on neutrinos from the ^{8}B channel is discussed. We summarize our results in Sect. 6.

2. Standard solar model

A SSM represents the mathematical way of fitting the present-day Sun status, provided some boundary conditions as luminosity, radius, mass, and composition are available. Other important features such as temperature, pressure, sound-speed profiles, solar photospheric abundances, and neutrino fluxes can then be predicted. Each of these quantities strictly depends on the nuclear reactions at work in the Sun's interiors, whose main outcome is helium production by hydrogen burning. This occurs through the pp-chain (~99%) and, to a much lesser extent, through the CN-cycle (~1%). Although the latter is not very important for the energy production in our Sun, it is relevant for the details of the neutrino production and as a test of the correctness of the predictions. Other ingredients of the input physics, such as equation of state (EoS), opacity, and chemical composition are also crucial for predicting the solar quantities mentioned above.

The essentials of a SSM include the full evolution of a 1 $M_\odot$ star from the pre-main sequence to the present solar age $t_\odot$ = 4.566 Gyr, usually by considering that mass loss is negligible. In addition, a SSM is required to reproduce, once the presolar composition is fixed, the present-day solar mass $M_\odot$, age, radius $R_\odot$, and luminosity $L_\odot$ as well as the observed metal-to-hydrogen ratio $(Z/X)_\odot$ at the surface of the Sun. In order to do this, in our models we calibrated accordingly, with an iterative procedure, the initial helium and metal mass fractions $Y_{\rm ini}$ and $Z_{\rm ini}$, respectively, as well as the mixing-length parameter ($\alpha_{\rm MLT}$). Our solar models have been calculated with the FUll Network Stellar evolution (FUNS) code (Straniero et al. 2006; Piersanti et al. 2007; Cristallo et al. 2011). All the models assume a present solar luminosity of $L_\odot = 3.8418 \times 10^{33}$ erg s^{-1}, a present solar radius $R_\odot = 6.9598 \times 10^{10}$ cm, and a solar mass $M_\odot = 1.989 \times 10^{33}$ g (Allen 1963; Bahcall et al. 2005a).

The input physics is basically the same adopted by Piersanti et al. (2007), but includes a few recent updates as listed below. We adopted the nuclear reaction rates presented in Table 1, except for the case of the ^{7}Be electron-captures, for which we used either the rate suggested by Adelberger et al. (2011) or that computed by Simonucci et al. (2013). Concerning the mean energy loss in the individual branches of neutrino production, we used the experimental values suggested by Vissani (2018; see their Table 2). For electron screening effects in the solar plasma we adopted the Salpeter formula for the weak-screening, as recommended by Gruzinov & Bahcall (1998) and Bahcall et al. (2002). The EoS is the same as that described by Straniero (1988) for fully ionized matter, in the form updated by Prada Moroni & Straniero (2002) for log T [K] ≥ 6.0 and a Saha equation for log T [K] < 6.0. Atomic diffusion has been included, taking into account the effects of gravitational settling and thermal diffusion, by inverting the coupled set of Burgers equations (Thoul et al. 1994; Piersanti et al. 2007). For radiative opacities, we used the OPAL tables (Iglesias & Rogers 1996) for high temperatures (log T [K] ≥ 4.0) and the Ferguson et al. (2005) molecular opacities for low temperatures (log T [K] < 4.0), corresponding to the scaled-solar composition given either by Grevesse & Sauval (1998) or by Palme et al. (2014; hereafter GS98 and PLJ14, respectively). Different choices of $(Z/X)_\odot$ correspond to different metal distributions in the solar structure, which, in their turn, change the calculated

Table 1. Major reaction rates included in the SSMs presented in this paper.

Reaction	Reference
^{1}H(p, $\beta^+\nu_e$)^{2}H	1
^{1}H(e$^-$p, ν_e)^{2}H	2
^{2}H(p, γ)^{3}He	2
^{3}He(p, $\beta^+\nu_e$)^{4}He	2
^{3}He(^{3}He, α)2H	2
^{3}He(α, γ)^{7}Be	2
^{7}Li(p, α)^{4}He	3
^{7}Be(p, γ)^{8}B	4
^{7}Be(e$^-$, ν_e)^{7}Be	2, 5
^{12}C(p, γ)^{13}N	2
^{13}C(p, γ)^{14}N	2
^{14}N(p, γ)^{15}O	6
^{15}N(p, γ)^{16}O	2
^{15}N(p, α)^{12}C	2
^{16}O(p, γ)^{17}F	2
^{17}O(p, γ)^{18}F	7
^{17}O(p, α)^{14}N	8
^{14}C(p, γ)^{15}N	9
^{18}O(p, γ)^{19}F	10
^{18}O(p, α)^{15}N	11
^{19}F(p, γ)^{20}Ne	12
^{19}F(p, α)^{16}O	13
^{6}Li(p, γ)^{7}Be	12
^{6}Li(p, ^{3}He)^{4}He	12
^{9}Be(p, γ)^{10}B	12
^{9}B(p, α)^{6}Li	14
^{10}B(p, γ)^{11}C	12
^{10}B(p, α)^{7}Be	14
^{11}B(p, γ)^{12}C	12
^{11}B(p, $\alpha\alpha$)^{4}He	12
^{14}C(β^-, $\bar{\nu}_e$)^{14}N	15
^{18}F(β^+, ν_e)^{18}O	16
^{18}O(β^-, $\bar{\nu}_e$)^{18}F	16

References. (1) Marcucci et al. (2013); (2) Adelberger et al. (2011); (3) Lamia et al. (2012); (4) Zhang et al. (2015); (5) Simonucci et al. (2013); (6) Marta et al. (2011); (7) Di Leva et al. (2014); (8) Bruno et al. (2016); (9) Iliadis et al. (2010); (10) Buckner et al. (2012); (11) La Cognata et al. (2010); (12) Angulo et al. (1999); (13) Indelicato et al. (2017); (14) Lamia et al. (2015); (15) Rauscher & Thielemann (2000); (16) Oda et al. (1994).

depth of the convective zone. Indeed, it was pointed out that SSMs with low metal abundances (i.e., with low $(Z/X)_\odot$ values) disagree with the helioseismologically measured sound speed, the depth of the convective zone, and the surface helium abundance (see, e.g., Bahcall et al. 2004). Solving this disagreement, known as the "solar abundance problem", is an issue not related to ^{7}Be decay and is therefore beyond the scope of this work. We show that the effects of using the new rate are independent from the solar mixture assumed and can be stated in a general way.

Finally, we have to mention that all the analyses presented in the various cases of this work were performed by keeping all the physical parameters fixed, except for the ^{7}Be electron-capture rate, to evaluate the specific role of this rate and to minimize the effects related to other inputs. The results obtained with the updated estimate of the ^{7}Be electron-capture rate given by STPB13 were compared with those obtained with the evaluation given by ADE11 for the two mentioned stellar choices of the chemical composition. In principle, different assumptions for the composition, i.e., for the metal abundances, may lead to differences in the solar core temperature, hence also in the solar structure and in neutrino fluxes; see Sect. 4 for a quantitative discussion.

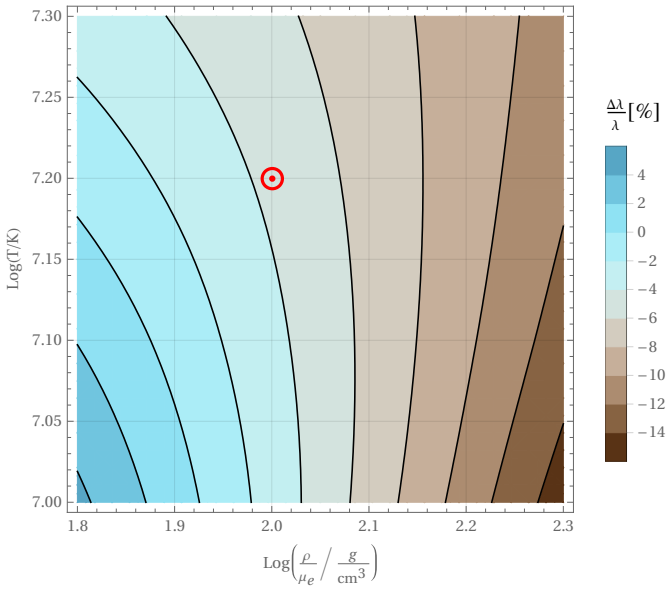

Fig. 1. Fractional variation of the ^{7}Be electron-capture rate, $\Delta\lambda/\lambda\,[\%] = 100 \cdot (R_{\mathrm{STPB13}} - R_{\mathrm{ADE11}})/R_{\mathrm{ADE11}}$, as a function of ρ/μ_e and T, adopting the Simonucci et al. (2013) rate, as compared to that of Adelberger et al. (2011) for the PLJ14 solar composition (see Sect. 2). The solar core conditions are highlighted with the common solar symbol.

3. Electron-capture on ^{7}Be

The deep stellar interiors are characterized by high densities and high temperatures. This implies that atoms are almost completely ionized; therefore, when describing the stellar core matter, it is necessary to apply the methods of plasma physics. The radioactive decay of a particular radioisotope (and its mean lifetime τ) is strongly dependent in such plasma conditions on the density ρ and temperature T of the plasma itself. In short, to provide an estimate of decay rates in stellar conditions we have to rely on accurate models for the plasma.

Many contributions, developed between the 1960s and 1980s, considered a ionized plasma, whose degree of ionization is described through the Saha equation. Free electrons, acting as a screen inside the Debye radius, are treated as a Maxwellian gas (Takahashi & Yokoi 1987). Concerning the specific case of ^{7}Be electron-captures, the first detailed calculation from continuum states was done by Bahcall (1962). Subsequently, estimates of the bound-electron contributions were also made (Iben et al. 1967; Bahcall & Moeller 1969; Bahcall 1994). A recommended resulting rate, based on all these calculations, was proposed by Adelberger et al. (1998) and Adelberger et al. (2011). More general treatments have also been developed over the years (Gruzinov & Bahcall 1997; Brown & Sawyer 1997; Sawyer 2011), but always referring to solar core conditions and maintaining an approach resembling the Born–Oppenheimer (BO) one. In addition to this, it was recognized that the major uncertainty affecting the decay rate arises from possible deviations from a pure Debye screening. Indeed, Johnson et al. (1992) estimated these possible corrections to the Debye–Hückel (DB) approximation by means of self-consistent thermal Hartree calculations, concluding that the proposed rate was correct within an accuracy of about 2%. In this regard, it has to be remarked that the temperature at the center of the Sun ($T \simeq 15.5$ MK) is too high for electron degeneracy to set in. Hence, the classical approximation used, for example, by Bahcall to derive his rate is well founded for the solar conditions.

Recently, Simonucci et al. (2013) developed a first-principles approach to derive the ^{7}Be electron-capture rate by modeling the electron-capture as a two-body scattering process ^{7}Be-e$^-$. To this aim, the e$^-$-capture process is assumed to be proportional to the electronic density at the nucleus $\rho_e(0)$, which is screened and modified by the presence of the surrounding particles. We notice in passing that the DB approximation used by Bahcall represents the high-temperature classical limit of the approach developed by Simonucci et al. (2013), which provides the e$^-$-capture rate on ^{7}Be over a range of plasma densities and temperatures definitively wider than that in the solar core conditions.

In this approach, the plasma is assumed hot and is modeled as a homogeneous *Fermi* gas made by ^{7}Be atoms, surrounded by N_p protons (hydrogen nuclei) and N_e electrons, at various temperatures T and densities ρ. The motion of quantum Fermi gases is ruled by the Schrödinger equation and described in a reference frame fixed on the Be nucleus. Because of the adopted non-inertial frame, the Hamiltonian of the system contains non-inertial terms, coupling the motion of particles of the different species. As Be is definitively more massive, all these terms can be safely neglected, so that a factorization of the eigenfunctions can be performed and separable eigensolutions can be found. This procedure is reminiscent of the conditions for the adiabatic theorem, and thus it represents an adiabatic approximation. In this way the many-body scattering problem is reduced to a screened two-body problem. As such, $\rho_\mathrm{e}(0)$ is computed by solving a coupled Hartree–Fock (HF) self-consistent system of equations for both protons and electrons in the electric field generated by a ^{7}Be nucleus located at the origin of the reference frame. The HF treatment of the Coulomb repulsion is satisfactory and accurate enough to comply with the electron correlation in stellar conditions (see Simonucci et al. 2013).

The mean lifetime, resulting from this method, is in general compatible with estimates by Bahcall (1962, 1994), Bahcall & Moeller (1969), and Adelberger et al. (1998, 2011); however, the mean lifetime has values that in solar conditions are smaller by ∼3–4% with respect to those estimated in the mentioned works. Far from these conditions, the differences can be much more pronounced (see Fig. 1). Details of the calculations

Table 2. Coefficients for the analytical approximation to the STPB13 and ADE11 electron-capture rates.

	κ	α	β	γ
This paper	5.9065×10^{-9}	-1.3614×10^{-2}	-9.2042×10^{-4}	-1.5334×10^{-1}
ADE11	5.6×10^{-9}	$+4 \times 10^{-3}$	0	0

are provided in Simonucci et al. (2013). The total reaction rate λ for ^{7}Be(e$^-$,ν_e)^{7}Li by STPB13 can also be expressed analytically in an approximate formula, as a function of temperature, density, and composition.

An expression that agrees with an accuracy of 2% to the tabulated results for the rate λ [s^{-1}], in the region of relevance for solar physics, i.e., $35 \lesssim \rho/\mu_e$ [g cm^{-3}] $\lesssim 105$ and $10 \leq T_6$ [MK] ≤ 16, is written as

$$\lambda(\frac{\rho}{\mu_e}, T_6) = \frac{\rho}{\mu_e}\frac{\kappa}{\sqrt{T_6}}\Big[1+\alpha\,(T_6-16)+\beta\,\frac{\rho}{\mu_e}\,\Big(1+\gamma\,(T_6-16)\Big)\Big]. \quad (1)$$

In this equation, μ_e is the mean molecular weight per electron, T_6 is the temperature in units of 10^6 K, and ρ is the density in units of [g cm^{-3}]. Thus, the electron density is $n_e = \rho/(m_p\mu_e)$, where m_p is the proton mass. The values of the four coefficients $\kappa, \alpha, \beta, \gamma$, whose units ensure the correct dimension of Eq. (1), are reported in Table 2. We notice that a nonlinear term in the density is present, while it was absent in Bahcall's calculations. In fact, this term results from the Coulomb repulsion (electron screening) acted upon the electrons, which modifies the density close to the nucleus. Taking into account such a nonlinearity requires the introduction of a higher number of polynomial terms. We recall, however, that in this work we make use of a tabulated version of the decay rate by STPB13: in fact, the adopted fine resolution allows us to compute highly accurate solar models without adding further uncertainties deriving from the use of an analytical formula. We note that in our discussion, none of the nuclear reaction rates relevant for the standard solar model has been modified, so that expected variations are entirely a consequence of the new approach adopted in computing ^{7}Be electron-capture rate. Nevertheless, the change in the electron density, due to the formalism introduced by Simonucci et al. (2013) to describe e$^-$-capture on ^{7}Be, might also be relevant for other charged-particle interactions, leading to a correction in the screening factor. An investigation of this possibility and the quantitative estimation of this effect deserves dedicated analyses and future work.

4. Solar neutrino fluxes

Stars with initial mass $M \lesssim 1.2\,M_\odot$ primarily burn hydrogen through the pp-chain. The latter has three main branches, namely the ppI-, ppII-, and ppIII-cycles. The pp, ^{8}B β-decay, and hep reactions produce neutrino spectra with characteristic shapes and with energies from zero up to a maximum energy q. In particular, the neutrinos coming from the weak hep branch are the most energetic neutrinos produced by the Sun ($q \leq 18.773$ MeV) and, thus, are observed in the SNO and Super-Kamiokande event distributions because they populate energy bins above the ^{8}B neutrino endpoint. The electron-capture reactions p + e$^-$ + p and ^{7}Be + e$^-$ produce, on the contrary, emission lines, possibly broadened by thermal effects. Concerning the ^{7}Be neutrinos, they form two distinct lines, corresponding to population of both the ground state (89.5%) and the first excited state (10.5%) in ^{7}Li (Vissani 2018).

The ppI, ppII, and ppIII contributions to solar energy generation can be determined from measurements of the pp/pep, ^{7}Be, and ^{8}B neutrino fluxes. Because the relative rates are very sensitive to the solar core temperature T_c, it is possible to infer important information about the physics of the solar interior from neutrino fluxes. Nowadays the pp, ^{7}Be, and ^{8}B fluxes are well known, while the measured pep neutrino flux is strongly model-dependent. In particular, this flux depends on the metallicity assumed for estimating the competing CNO neutrinos (Agostini et al. 2018). The solar core physics is sensitive to metallicity effects because of the free-bound/bound-free transitions in metals, which are important contributors to the opacity. This means that metallicity variations alter the solar core temperature and, in turn, the fluxes of temperature-sensitive neutrinos, such as those from ^{8}B β-decay. Heavier metals (Mg, Si, and Fe) also affect the predicted neutrino fluxes (see Bahcall et al. 1982). Even if not very abundant, they are important opacity sources at the Sun center, as they are highly ionized. Instead, in the region just below the convective zone, at temperatures of a few millions kelvins, they are small contributors to the opacity. On the contrary, abundant, lighter, volatile heavy elemements (C, N, O, Ne, and Ar) are partially ionized there and significantly affect the radiative opacities. This is the origin of discrepancies between helioseismological measurements and the predictions made using solar compositions with low (Z/X), as discussed in Bahcall et al. (2005b) and Bahcall & Serenelli (2005). As a matter of fact, abundance variations of different metals influence different regions in the solar interior. Moreover, different CNO abundances also imply an effect on CNO burning efficiency (and corresponding neutrino fluxes) and a minor effect on the mean molecular weight and, in turn, on the thermodynamical quantities.

The net effect is that models using the GS98 compilation of abundances exhibit higher temperatures and higher densities

Table 3. Main relevant quantities for the solar models adopting the ADE11 rate, as defined in the text.

	GS98	PLJ14
$R_{CE}/R_\odot$	0.71628	0.72294
T_c [10^7 K]	1.55031	1.54286
ρ_c [g cm^{-3}]	149.377	148.325
α_{MLT}	2.31832	2.30317
X_{ini}	0.70428	0.71092
Y_{ini}	0.27703	0.27256
Z_{ini}	0.01868	0.01653
$(Z/X)_{ini}$	0.02653	0.02325
$X_\odot$	0.73656	0.74412
$Y_\odot$	0.24656	0.24103
$Z_\odot$	0.01688	0.01485
$(Z/X)_\odot$	0.02292	0.01995

Notes. The models using the STPB13 rate show negligible variations for the same quantities. The value R_{CE} is the radius at the base of the convective envelope, T_c and ρ_c are the central temperature and density, and α_{MLT} is the value of the mixing-length parameter. The values X_{ini}, Y_{ini}, Z_{ini} and $(Z/X)_{ini}$ are the initial hydrogen, helium and metal abundances by mass and the initial metal-to-hydrogen ratio, while $X_\odot$, $Y_\odot$, $Z_\odot$ and $(Z/X)_\odot$ are the corresponding present-day photospheric values.

Table 4. Predicted fluxes in units of 10^{10} (pp), 10^9 (^{7}Be), 10^8 (pep, ^{13}N, ^{15}O), 10^6 (^{8}B, ^{17}F), and 10^3 (hep) cm^{-2} s^{-1} for the reference ADE11 models, presented in Table 3, for the STPB13 models and relative differences.

	GS98			PLJ14		
	ADE11	STPB13	Relative differences	ADE11	STPB13	Relative differences
Φ(pp)	5.99	5.99	+0.20‰	6.01	6.01	+0.01‰
Φ(pep)	1.42	1.42	+0.25‰	1.43	1.43	+0.01‰
Φ(hep)	8.09	8.09	+0.15‰	8.22	8.22	+0.01‰
Φ(^{7}Be)	4.74	4.74	+0.38‰	4.54	4.54	−0.01‰
Φ(^{8}B)	5.28	5.42	+2.70%	4.82	4.95	+2.60%
Φ(^{13}N)	2.82	2.82	+0.67‰	2.55	2.55	+0.06‰
Φ(^{15}O)	2.07	2.07	+0.71‰	1.82	1.82	+0.07‰
Φ(^{17}F)	5.35	5.35	+0.80‰	3.95	3.95	+0.07‰

with respect to those using that of PLJ14 (see Table 3). On the other hand, while pp and pep fluxes are only slightly modified, ^{7}Be, ^{8}B, ^{13}N, ^{15}O, and ^{17}F neutrino fluxes are rather enhanced. Their fluxes are indeed strongly dependent on the central temperature T_c, with a power law of the form $\Phi \propto T_c^m$, where m = 10.0, 24.0, 24.4, 27.1, and 27.8, respectively (see Bahcall & Ulmer 1996). CNO neutrino fluxes are also enhanced because of the increased burning efficiency caused by the higher CNO abundances in the GS98 compilation. As was already mentioned, using modern solar compositions such as that of PLJ14, with low surface metal abundances, solar models have been found to be in disagreement with helioseismological measurements (see Bahcall et al. 2004, 2005a; Basu & Antia 2004; Serenelli et al. 2011; Haxton et al. 2013; Vinyoles et al. 2017). We checked that the predicted sound speed profiles of our computed SSMs are in agreement with others in the literature. We found that for the PLJ14 abundance choice the prediction disagrees with that measured (Schou et al. 1998). Instead, the choice of the older GS98 composition gives a better match.

We recall however that this work is not aimed at giving the best prediction for the total neutrino fluxes nor at probing the solar metallicity problem, rather we want to probe the effects induced on solar neutrino fluxes by varying the ^{7}Be electron-capture rate alone, in the light of the mentioned evaluation by STPB13.

5. Impact of a revised ^{7}Be + e$^-$ on the ^{8}B neutrino flux

In this section we want to evaluate the impact of using a revised rate for the ^{7}Be electron-capture, computed following the approach suggested by Simonucci et al. (2013), on the ^{8}B neutrino flux. While pp neutrinos originate in a wide range of the Sun, corresponding to the main energy-producing region, ^{7}Be and ^{8}B neutrinos are produced in a hotter and narrower zone, ranging from the solar center to about 0.15–0.2 $R_\odot$. The quantities $R_{\rm STPB13}$ and $R_{\rm ADE11}$ represent the electron-capture rate given by STPB13 and by ADE11, respectively. As shown in the top panel of Fig. 2, there is an appreciable variation: the new rate is lower with respect to the ADE11 choice in solar core conditions, meaning that the ^{7}Be neutrino production channel is slightly suppressed in favor of all other channels. In particular, the solar neutrino fluxes from ^{7}Be and ^{8}B, Φ(^{7}Be) and Φ(^{8}B) are proportional to the local density of ^{7}Be ions. The Φ(^{7}Be) flux depends on both the electron-capture ($R_{\rm ec}$) and the proton-capture rate ($R_{\rm pc}$) through

$$\Phi(^7\mathrm{Be}) \propto \frac{R_{\rm ec}}{R_{\rm ec} + R_{\rm pc}}\,, \tag{2}$$

where $R_{\rm pc} \approx 10^{-3}\ R_{\rm ec}$ (see Adelberger et al. 1998). The flux Φ(^{7}Be) is therefore basically independent from the rates and dependent only upon the branching ratio of the reactions ^{3}He+^{3}He e ^{3}He+^{4}He. On the contrary, Φ(^{8}B) can be written as

$$\Phi(^8\mathrm{B}) \propto \frac{R_{\rm pc}}{R_{\rm ec} + R_{\rm pc}} \simeq \frac{R_{\rm pc}}{R_{\rm ec}}\,, \tag{3}$$

meaning that it is inversely proportional to the electron-capture rate $R_{\rm ec}$. This means that a variation of the $R_{\rm ec}$ should have a linear effect on neutrino flux of ^{8}B and negligible effects on other channels. Indeed, the STPB13 models present exactly the same physical and chemical features of the ADE11 models (see Table 3). If we take into account neutrinos that originate in each fraction of the solar radius (Fig. 2, middle panel), we thus deduce that the ^{8}B neutrino production channel becomes more efficient and so Φ(^{8}B) is increased because of the less efficient electron-capture on ^{7}Be rate. It is also possible to see that, in correspondence of a change from negative to positive values of the variations in the electron-capture rate, the neutrino flux variation shifts from positive to negative values, thus corroborating the hypothesis of linearity between the electron-capture rate on ^{7}Be and the ^{8}B neutrino flux. Furthermore, if relation Eq. (3) holds, then we see that

$$\frac{n_\nu(^8\mathrm{B})_{\rm STPB13}}{n_\nu(^8\mathrm{B})_{\rm ADE11}} = \frac{\Phi(^8\mathrm{B})_{\rm STPB13}}{\Phi(^8\mathrm{B})_{\rm ADE11}} \simeq \frac{R_{\rm ADE11}}{R_{\rm STPB13}}, \tag{4}$$

or alternatively,

$$\frac{n_\nu(^8\mathrm{B})_{\rm STPB13}}{n_\nu(^8\mathrm{B})_{\rm ADE11}} \frac{R_{\rm STPB13}}{R_{\rm ADE11}} \simeq 1, \tag{5}$$

where n_ν(^{8}B) is the number of neutrinos coming from the ^{8}B decay. The bottom panel of Fig. 2 shows the product in the left-hand side of relation Eq. (5). Its value is consistent with unity at less than one part per thousand, meaning that relation Eq. (3) is indeed valid and that an increase of the $R_{\rm ec}$ has the effect of linearly decreasing the flux of ^{8}B neutrinos. Finally, variations by +2.6% and +2.7% in Φ(^{8}B) are obtained for SSMs using a PLJ14 or a GS98 composition, respectively (see Table 4). The adoption of the STPB13 rate for electron-captures on ^{7}Be has

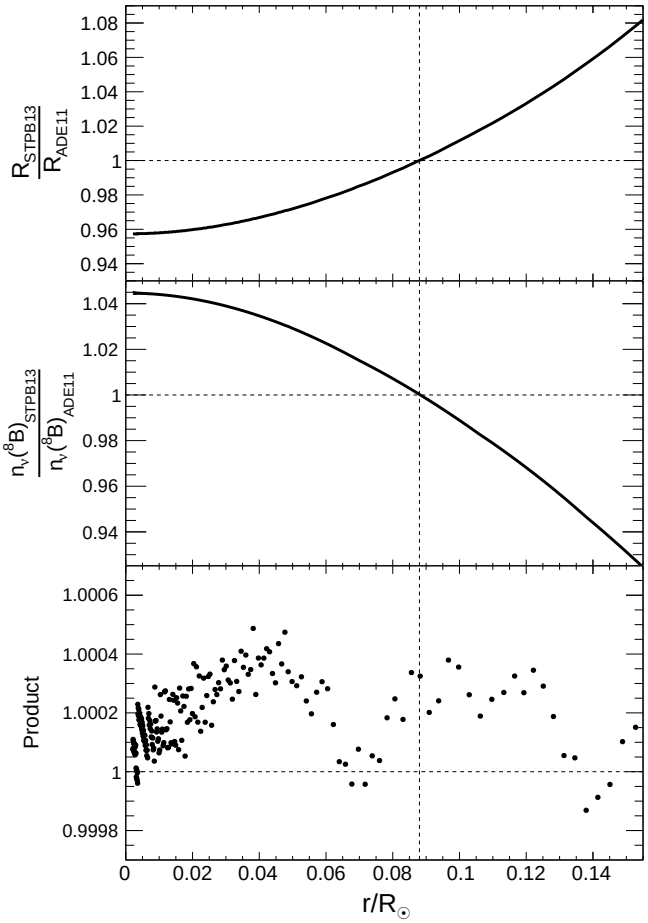

Fig. 2. *Top panel*: ratio of the STPB13 electron-capture rate to that of ADE11 in the production region of ^{8}B neutrinos. These are both computed on the solar structure resulting from the ADE11 SSM, with a PLJ14 composition. *Middle panel*: ratio of the neutrinos fraction produced in STPB13 SSM to that of ADE11, both computed with a PLJ14 composition. *Bottom panel*: product $n_\nu(^8\mathrm{B})_{\mathrm{STPB13}} \cdot R_{\mathrm{STPB13}} / \left(n_\nu(^8\mathrm{B})_{\mathrm{ADE11}} \cdot R_{\mathrm{STPB13}}\right)$ is shown; we note, in comparison with the other two panels, the much finer vertical scale. The consistency of this value with the unity means that there is practically no difference in computing a SSM with the revised STPB13 rate or applying it directly on the solar structure of a ADE11 SSM.

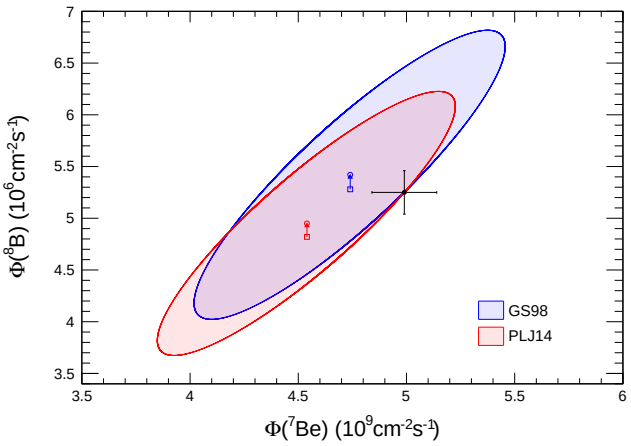

Fig. 3. Fluxes of $\Phi(^8\mathrm{B})$ and $\Phi(^7\mathrm{Be})$ compared to solar values (Aharmim et al. 2013; Agostini et al. 2018). The black dot and error bars indicate solar values, while the squares and circles indicate the results obtained with the ADE11 electron-capture rate (older) and that of STPB13 (current), respectively. Ellipses denote theoretical 1σ confidence level (C.L.) for 2 degrees of freedom.

negligible effects on all other neutrino fluxes because it induces no variation on the physics and chemistry of the SSM itself (see Table 3).

At the present moment we cannot tag our predicted fluxes with well-defined uncertainty estimates. We should construct Monte Carlo (MC) simulations of SSMs to provide statistical errors to our results (see Bahcall et al. 2006; Serenelli et al. 2011; Vinyoles et al. 2017). Still we can estimate these uncertainties starting from known literature. Concerning the predicted ^{8}B neutrino flux, Bahcall et al. (2006) found that the 1σ theoretical uncertainty varies from 17% to 11%, depending on the adopted composition (see their Table 15 and Fig. 6). Similar but lower values were also found by Serenelli et al. (2011) and Vinyoles et al. (2017). Then we can choose, in a conservative way, the higher value of 17% as our uncertainty on the predicted ^{8}B neutrino flux. Similarly we can adopt an error of 10% 1σ on the ^{7}Be neutrino flux, as predicted by Bahcall et al. (2006), which is the highest found in the literature. We also use, as correlation coefficient of the ^{7}Be-^{8}B neutrino fluxes, that given by Bahcall et al. (2006) for the GS98 composition. In this way we only give a rough, but still reliable, estimate of the uncertainties affecting our neutrino flux predictions, to be compared with the measured values.

The final joint fit to all SNO data gave a total flux of neutrino from ^{8}B decays in the Sun of $\Phi(^8\mathrm{B}) = 5.25(1 \pm 0.04) \times 10^6\,\mathrm{cm}^{-2}\,\mathrm{s}^{-1}$ (Aharmim et al. 2013). The latest results of the Borexino collaboration (Agostini et al. 2018) provided a total flux of ^{7}Be neutrino flux of $\Phi(^7\mathrm{Be}) = 4.99(1 \pm 0.03) \times 10^9\,\mathrm{cm}^{-2}\,\mathrm{s}^{-1}$. Such a value is somehow model-dependent, being obtained from the measured rates assuming a specific mechanism of neutrino oscillations (see Agostini et al. 2018, for details). In fact, elastic scattering measurements, such as those performed by Borexino, are mainly sensitive to ν_e charged-current interactions. On the contrary, the neutral-current detection channel in SNO is sensitive to all neutrino flavors and so it is a direct model-independent observation of the ^{8}B solar neutrino flux. Figure 3 shows that adopting either the GS98 or PLJ14 compositions leads to a fair agreement with the total ^{8}B neutrino flux measured by the SNO neutral current experiments. The use of the revised electron-capture rate R_{STPB13} increases the old values of the predicted ^{8}B neutrino fluxes with respect to the measured value. The measured value of the ^{8}B neutrino flux is compatible with the solar model predictions for each of the two adopted solar compositions.

6. Conclusions

We have presented new SSMs for two different mixtures of solar abundances, GS98 and PLJ14. We performed the simulation with the FUNS code suite. We used recent values for the cross sections in our nuclear reaction network. In particular, we adopt the e$^-$-capture rate on ^{7}Be provided by Simonucci et al. (2013) based on a description of the physical conditions in the solar interior that is more accurate than previous works (e.g., ADE11) and is also applicable to more general stellar environments. A tabulated version of this rate is available at the CDS. The comparison with models computed with the ADE11 widely adopted electron-capture rate shows maximum differences of about 3–4% in solar conditions. The effects on the standard solar model calculations, along with the effects on neutrino fluxes, have been discussed. We found that variations in the solar structure and in

neutrino fluxes are negligible, except for the ^{8}B neutrino flux. The estimated increase is 2.6–2.7%, depending on the composition assumed. Finally, we have also shown that the solar ^{8}B neutrino flux is reproduced rather well, both using the GS98 and PLJ14 abundance sets.

Acknowledgements. We warmly thank the referee, S. Degl'Innocenti, for the insightful comments and suggestions that helped us to improve the manuscript.

References

Abe, K., Haga, Y., Hayato, Y., et al. 2016, Phys. Rev. D, 94, 052010
Adelberger, E. G., Austin, S. M., Bahcall, J. N., et al. 1998, Rev. Mod. Phys., 70, 1265
Adelberger, E. G., García, A., Robertson, R. G. H., et al. 2011, Rev. Mod. Phys., 83, 195
Agostini, M., Altenmüller, K., Appel, S., et al. 2018, Nature, 562, 505
Aharmim, B., Ahmed, S. N., Anthony, A. E., et al. 2013, Phys. Rev. C, 88, 025501
Allen, C. W. 1963, Astrophysical Quantities (London: University of London, Athlone Press)
Angulo, C., Arnould, M., Rayet, M., et al. 1999, Nucl. Phys. A, 656, 3
Asplund, M. 2005, ARA&A, 43, 481
Bahcall, J. N. 1962, Phys. Rev., 126, 1143
Bahcall, J. N. 1994, Phys. Rev. D, 49, 3923
Bahcall, J. N., & Moeller, C. P. 1969, ApJ, 155, 511
Bahcall, J. N., & Serenelli, A. M. 2005, ApJ, 626, 530
Bahcall, J. N., & Ulmer, A. 1996, Phys. Rev. D, 53, 4202
Bahcall, J. N., Huebner, W. F., Lubow, S. H., Parker, P. D., & Ulrich, R. K. 1982, Rev. Mod. Phys., 54, 767
Bahcall, J. N., Pinsonneault, M. H., & Basu, S. 2001, ApJ, 555, 990
Bahcall, J. N., Brown, L. S., Gruzinov, A., & Sawyer, R. F. 2002, A&A, 383, 291
Bahcall, J. N., Serenelli, A. M., & Pinsonneault, M. 2004, ApJ, 614, 464
Bahcall, J. N., Basu, S., Pinsonneault, M., & Serenelli, A. M. 2005a, ApJ, 618, 1049
Bahcall, J. N., Serenelli, A. M., & Basu, S. 2005b, ApJ, 621, L85
Bahcall, J. N., Serenelli, A. M., & Basu, S. 2006, ApJS, 165, 400
Basu, S., & Antia, H. M. 2004, ApJ, 606, L85
Brown, L. S., & Sawyer, R. F. 1997, ApJ, 489, 968
Bruno, C. G., Scott, D. A., Aliotta, M., et al. 2016, Phys. Rev. Lett., 117, 142502
Buckner, M. Q., Iliadis, C., Cesaratto, J. M., et al. 2012, Phys. Rev. C, 86, 065804
Cristallo, S., Piersanti, L., Straniero, O., et al. 2011, ApJS, 197, 17
Di Leva, A., Scott, D. A., Caciolli, A., et al. 2014, Phys. Rev. C, 89, 015803
Ferguson, J. W., Alexander, D. R., Allard, F., et al. 2005, ApJ, 623, 585
Grevesse, N., & Sauval, A. J. 1998, Space Sci. Rev., 85, 161
Gruzinov, A. V., & Bahcall, J. N. 1997, ApJ, 490, 437
Gruzinov, A. V., & Bahcall, J. N. 1998, ApJ, 504, 996
Haxton, W., Robertson, R. H., & Serenelli, A. M. 2013, ARA&A, 51, 21
Iben, Jr., I., Kalata, K., & Schwartz, J. 1967, ApJ, 150, 1001
Iglesias, C. A., & Rogers, F. J. 1996, ApJ, 464, 943
Iliadis, C., Longland, R., Champagne, A. E., Coc, A., & Fitzgerald, R. 2010, Nucl. Phys. A, 841, 31
Indelicato, I., La Cognata, M., Spitaleri, C., et al. 2017, ApJ, 845, 19
Johnson, C. W., Kolbe, E., Koonin, S. E., & Langanke, K. 1992, ApJ, 392, 320
La Cognata, M., Spitaleri, C., & Mukhamedzhanov, A. M. 2010, ApJ, 723, 1512
Lamia, L., Spitaleri, C., La Cognata, M., Palmerini, S., & Pizzone, R. G. 2012, A&A, 541, A158
Lamia, L., Spitaleri, C., Tognelli, E., et al. 2015, ApJ, 811, 99
Marcucci, L. E., Schiavilla, R., & Viviani, M. 2013, Phys. Rev. Lett., 110, 192503
Marta, M., Formicola, A., Bemmerer, D., et al. 2011, PhRvC, 83, 045804
Oda, T., Hino, M., Muto, K., Takahara, M., & Sato, K. 1994, At. Data Nucl. Data Tables, 56, 231
Palme, H., Lodders, K., & Jones, A. 2014, Solar System Abundances of the Elements, ed. A. M. Davis, 15
Piersanti, L., Straniero, O., & Cristallo, S. 2007, A&A, 462, 1051
Prada Moroni, P. G., & Straniero, O. 2002, ApJ, 581, 585
Rauscher, T., & Thielemann, F.-K. 2000, At. Data Nucl. Data Tables, 75, 1
Sawyer, R. F. 2011, Phys. Rev. C, 83, 065804
Schou, J., Antia, H. M., Basu, S., et al. 1998, ApJ, 505, 390
Serenelli, A. M., Haxton, W. C., & Peña-Garay, C. 2011, ApJ, 743, 24
Simonucci, S., Taioli, S., Palmerini, S., & Busso, M. 2013, ApJ, 764, 118
Straniero, O. 1988, A&AS, 76, 157
Straniero, O., Gallino, R., & Cristallo, S. 2006, Nucl. Phys. A, 777, 311
Takahashi, K., & Yokoi, K. 1987, ADNDT, 36, 375
Thoul, A. A., Bahcall, J. N., & Loeb, A. 1994, ApJ, 421, 828
Vinyoles, N., Serenelli, A. M., Villante, F. L., et al. 2017, ApJ, 835, 202
Vissani, F. 2018, ArXiv e-prints [arXiv:1808.01495]
Zhang, X., Nollett, K. M., & Phillips, D. R. 2015, Phys. Lett. B, 751, 535